Nonlinear spin conductance of yttrium iron garnet thin films driven by large spin-orbit torque

N. Thiery, A. Draveny, V. V. Naletov, L. Vila, J. P. Attané, C. Beigné, G. de Loubens, M. Viret, N. Beaulieu, J. Ben Youssef, V. E. Demidov, S. O. Demokritov, A. N. Slavin, V. S. Tiberkevich, A. Anane, P. Bortolotti, V. Cros, and O. Klein

Spin nonlinear conductance of YIG thin films driven by large spin-orbit torque

N. Thiery,[1] A. Draveny,[1] V. V. Naletov,[1, 2] L. Vila,[1] J.P. Attané,[1] C. Beigné,[1] G. de
Loubens,[3] M. Viret,[3] N. Beaulieu,[3, 4] J. Ben Youssef,[4] V. E. Demidov,[5] S. O. Demokritov,[5, 6]
A. N. Slavin,[7] V. S. Tiberkevich,[7] A. Anane,[8] P. Bortolotti,[8] V. Cros,[8] and O. Klein[1, *]

[1] SPINTEC, CEA-Grenoble, CNRS and Université Grenoble Alpes, 38054 Grenoble, France
[2] Institute of Physics, Kazan Federal University, Kazan 420008, Russian Federation
[3] SPEC, CEA-Saclay, CNRS, Université Paris-Saclay, 91191 Gif-sur-Yvette, France
[4] LabSTICC, CNRS, Université de Bretagne Occidentale, 29238 Brest, France
[5] Department of Physics, University of Muenster, 48149 Muenster, Germany
[6] Institute of Metal Physics, Ural Division of RAS, Yekaterinburg 620041, Russian Federation
[7] Department of Physics, Oakland University, Michigan 48309, USA
[8] Unité Mixte de Physique CNRS, Thales, Université Paris-Saclay, 91767 Palaiseau, France
(Dated: February 9, 2018)

We report high power spin transfer studies in open magnetic geometries, by measuring the spin conductance between two nearby Pt wires deposited on top of an epitaxial Yttrium Iron Garnet (YIG) thin film. Spin transport is provided by propagating spin waves, that are generated and detected by direct and inverse spin Hall effects. We observe a crossover in spin conductance from a linear transport dominated by exchange magnons (low current regime), to a nonlinear transport dominated by magnetostatic magnons (high current regime). The latter are low-damping magnetic excitations, located near the spectral bottom of the magnon manifold, with a sensitivity to the applied magnetic field. This picture is supported by microfocus Brillouin Light Scattering spectroscopy. Our findings could be used for the development of controllable spin conductors by variation of relatively weak magnetic fields.
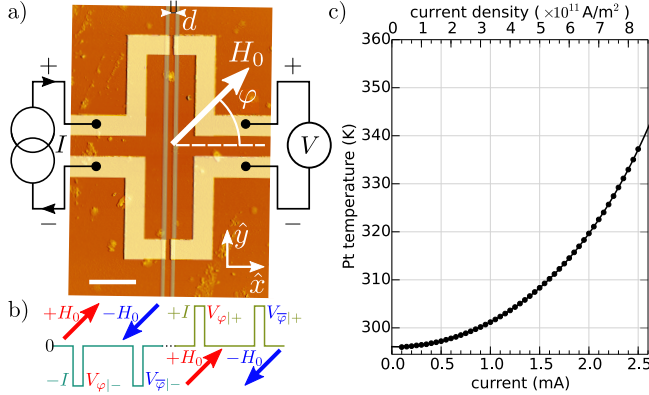
FIG. 1. (Color online) a) Top view of the lateral device. Two Pt wires (grey lines) are aligned along the $\hat{y}$-direction and placed at a distance $d = 1.2 \, \mu$m apart on top of a 18 nm thick YIG film (scale bar is 5 μm). The non-local conductance I-V (injector-detector) is measured using current pulses while rotating the magnetic field H_0 in-plane by an azimuthal angle φ. b) For each value of φ, 4 measurements of the voltage $V_{\varphi|I}$ are performed corresponding to the 4 combinations of the polarities of $H_0|I$. Panel c) shows the temperature elevation produced in the Pt injector by Joule heating while increasing the pulse amplitude I.

The recent demonstrations that spin orbit torques (SOT) allow one to generate and detect pure spin currents[1–7] has triggered a renewed effort to study magnons transport in magnetic insulators. A large effort has concentrated so far on yttrium iron garnet (YIG), which is famous for having the lowest known magnetic damping parameter. From a fundamental point of view, these studies of magnon transport in YIG by means of the direct and inverse spin Hall effects (ISHE)[2,8–18] are very interesting, as they provide new means to alter strongly the energy distribution of magnons up to thermal energies. The interplay between these non-equilibrium populations is expected to lead to new collective phenomena, even potentially, to trigger quantum condensation at room temperature[19].

Still now, very little is known about spin transfer processes in open geometries (size larger than the magnons propagation distance), which have continuous spin-wave (SW) spectra containing many modes which can take part in magnon-magnon interactions. While magnons excited coherently, e.g. by ferromagnetic resonance or parametric pumping have their frequencies fully determined by the the external signals, magnon excitation by spin transfer processes lacks frequency selectivity[20], and, therefore, can lead to their excitation in a broad frequency range. This poses a challenge for the identification of the nature of magnons modes excited by SOT. It has been already shown in[21], that it is convenient and useful to introduce the concepts of subthermal (having energy close to the bottom of the spin wave spectrum) and thermal (having energy close to $k_B T$) magnons. On one hand, it is well established[22,23] that subthermal magnons can be very efficiently thermalized near the spectral bottom (region of so-called magnetostatic waves) by the intensive nonlinear magnon-magnon interaction (here the decay rate between quasi-degenerate modes increases with power) to reach a quasi-equilibrium state by a non-zero chemical potential[22–24] and an effective temperature[25]. On the other hand, it is so far assumed that the groups of subthermal and thermal magnons are

effectively decoupled from each other, when one writes that the saturation magnetization, which implicitly accounts for the number of thermal magnons, is a conserved quantity of the motion in the gyromagnetic equation.

Under spin transfer processes, whose efficiency is known to increase with decreasing magnon frequency, in closed geometries (lateral size smaller than the magnons propagation distance, hereby leading to a quantized spectrum) it has been shown, that one can reach current induced coherent GHz-frequency magnon dynamics in YIG[15,16,26]). In open geometries, the recently discovered non-local magnon transport[8,9,27–29] suggests that the spin conductance of YIG films subjected to small SOT is instead dominated by magnons at thermal energy, whose number overwhelmingly exceeds the number of other modes at any finite temperature. The interesting challenge is to elucidate what will happen to this spectrum (in particular the interplay between thermal and subthermal population[30,31]) when one applies very large SOT to a magnon continuum.

We propose herein to measure the spin conductance of YIG films when the driving current is varied in a wide magnitude range creating, first, a quasi-equilibrium transport regime, and, then, driving the system to a strongly out-of-equilibrium state. To reach this goal the spin current density injected in the YIG by SOT shall be increased by more than one order of magnitude compared to previous works, while simultaneously reducing the film thickness by also an order of magnitude, using ultra-thin films of YIG. A series of lateral devices have been patterned on a 18 nm thick YIG films grown by liquid phase epitaxy[13,32]. Ferromagnetic resonance (FMR) characterization of the bare film are summarized in Table 1. On these films, we have deposited Pt wires, 10 nm thick, 300 nm wide, and 20 μm long. The lateral device geometry is shown in FIG.1a. One monitors the voltage V along one wire as a current I flows through a second wire separated by a gap of 1.2 μm. Here the Pt wires are connected by 50 nm thick Al electrodes colored in yellow. Thereafter, the transport studies will be performed in air and at room temperature (note that a protective layer of 20 nm of Si_3N_4 has been deposited over the top surface to prevent oxidation). Since a large amount of electrical current needs to flow in the Pt, a pulse method is used to reduce significantly Joule heating. In the following the current is injected during 10 ms pulses series enclosed in a 10% duty cycle. Temperature sensing is provided by the change of relative resistance of the Pt wire during the pulse. In FIG.1b, we have plotted $\kappa_{Pt}(R_I - R_0)/R_0$ as a function of the current I, where R_I and $R_0 = 1.3$ kΩ are respectively the electric resistance of Pt in the presence and absence of current, and the coefficient $\kappa_{Pt} = 254$ K is specific to Pt. We observe that the pulse method allows to keep the absolute temperature of YIG below 340 K[33] at the maximum current amplitude of 2.5 mA. Avoiding excessive heating of the YIG is crucial because, in a joint review paper[34], it is shown that our epitaxial YIG thin films behave as a large gap semiconductor, with an

TABLE I. Summary of the physical properties of the YIG thin film (YDPB8) and Pt used in this study.

t_{YIG} (nm)	$4\pi M_s$ (G)	α_{YIG}	ΔH_0 (Oe)	$\gamma(\mathrm{rad \cdot s^{-1} \cdot G^{-1}})$
18	1.6×10^3	4.4×10^{-4}	3.7	1.79×10^7

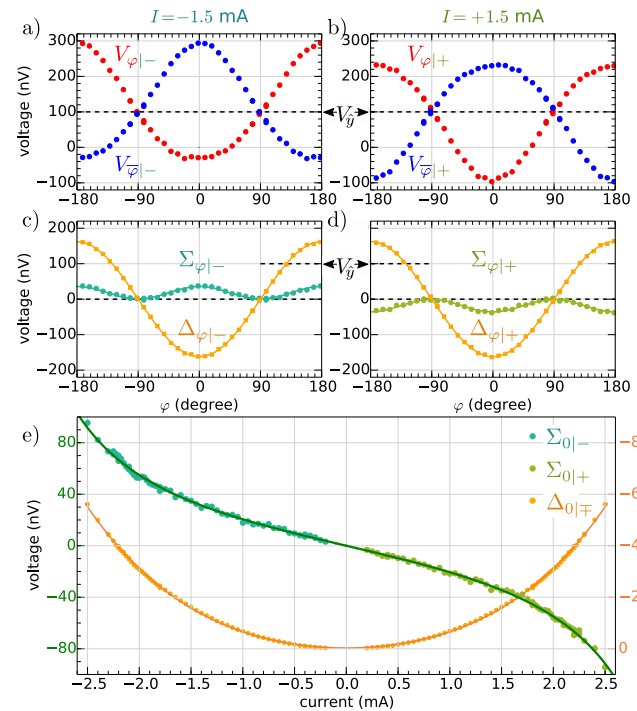| t_{Pt} (nm)	ρ_{Pt} ($\mu\Omega$.cm)	$\alpha_{YIG|Pt}$		$g_{\uparrow\downarrow}$ (m^{-2})
10	19.5	2.4×10^{-3}		3×10^{18}

FIG. 2. (Color online) Angular dependence of the non-local voltages $V_{\pm|\mp}$ measured while inverting the polarity of the applied field $H_0 = \pm 2$kOe (red/blue) respectively for a) negative and b) positive current pulses $I = \mp 1.5$mA. The measured signal can be decomposed c) and d) in three components: Σ (green): the signal sum, Δ (orange): the signal difference and $V_{\hat{y}}$: the offset; respectively even/odd, odd/even in field/current, and an angle independent contribution (dashed). Panel e) shows the current dependence of the amplitude Σ and Δ at $\varphi = 0$.

electrical resistivity that decreases exponentially with increasing temperature following an activated behavior. As shown in[34], at 340 K, however, the electrical resistivity of YIG remains larger than 10^6 $\Omega \cdot$cm and thus the YIG can still be considered a good insulator ($R > 30$ GΩ) over the current range explored herein.

The lateral device is biased by an in-plane magnetic field, H_0 set at a variable azimuthal angle φ (or its inverse $\overline{\varphi} = \varphi + 180°$) with respect to the x-axis (see FIG.1a). FIG.2a-d displays the results when $I = 1.5$ mA and $H_0 = 2$ kOe[35]. For each value of φ, 4 measurements $V_{\varphi|I}$ are performed corresponding to the 4 combinations of the polarities of $H_0|I$ (the polarity convention is defined in FIG.1a). FIG.2a and 2b show the raw data

obtained respectively for negative and positive current pulses. Clearly the non-local voltage oscillates around an offset, $V_{\hat{y}}$, defined as the voltage measured at $\varphi = \pm 90°$. This offset is ascribed to thermoelectric effects at the two Pt|Al contacts of the detector circuit, which are sensitive to any temperature gradient along the y-direction inherently produced by any resistance asymmetry along the Pt wire, which imbalances Joule heating (see discussion in[34]). By contrast, the anisotropic part of the voltage measured relatively to $V_{\hat{y}}$ is ascribed to magnons transport.

We now sort the non-local voltages (measured relatively to this offset $V_{\hat{y}}$) according to their symmetry with respect to the magnetization direction. We construct in FIG.2c and 2d the signal sum $\Sigma_\varphi = (V_\varphi - V_{\hat{y}})/2 + (V_{\overline{\varphi}} - V_{\hat{y}})/2$ (even with respect to the direction of the applied magnetic field, green) and the signal difference $\Delta_\varphi = (V_\varphi - V_{\hat{y}})/2 - (V_{\overline{\varphi}} - V_{\hat{y}})/2$ (odd with respect to the direction of the applied magnetic field, orange). This separation is exposed in their angular dependences, which follow two different behaviors, one in $\cos^2\varphi$, the other one in $\cos\varphi$, respectively. The solid lines in FIG.2c and 2d are fits by these two functions. As noticed in ref[8], these symmetries of Σ_φ and Δ_φ are the hallmark of respectively SOT[16] and spin Seebeck effects[36–38]. Hereafter, we shall use the fit of the whole angular dependence as a mean to extract precisely the amplitude of Σ_0 and Δ_0 at $\varphi = 0°$.

FIG.2e shows their evolution as a function of the current, I. One observes that $\Sigma_{0|I}$ is odd in current, while $\Delta_{0|I}$ is even in current, which are both the expected symmetry of SOT and of spin Seebeck effects with respect to current polarity. Importantly, this odd/even correspondence between the symmetries of $\Sigma_{0|I}$ and of $\Delta_{0|I}$ extends (within our measurement accuracy) on the whole current range. While $\Delta_{0|I}$ approximately follows the parabolic increase of the Pt temperature (cf. FIG.1a), as expected for thermal effects, the interesting novel feature is the fact that $\Sigma_{0|I}$ deviates from a purely linear transport behavior at large I. It is worthwhile also to emphasize that, when the high/low binding posts of the current source and voltmeter are biased in the same orientation (cf. FIG.1a), ($\Sigma_0 \cdot I$) is negative. This is a signature that the observed non-local voltage is produced by ISHE (see discussion in[34]). In the following, we shall concentrate exclusively on the nonlinear behavior of $\Sigma_{0|I}$ which measures the number of magnons created by SOT relatively to the number of magnons annhilated by SOT while being immune to spin current generated by Joule heating.

Using the same color code, we have plotted in FIG.3a both the variation of $\Sigma_{0|+}$ and $-\Sigma_{0|-}$ as a function of the current intensity. Since both quantities follow the same behavior on the whole current range, for the sake of simplicity we shall call simply $\Sigma = (\Sigma_{0|+} - \Sigma_{0|-})/2$ (dark green) their averaged. At low current, the SOT signal follows first a linear behavior $\Sigma^{(t)}/I = \partial\Sigma/\partial I|_{I=0}$ which is believed to be dominated by thermal magnons transport[8,39]. Quite remarkably the deviation from the
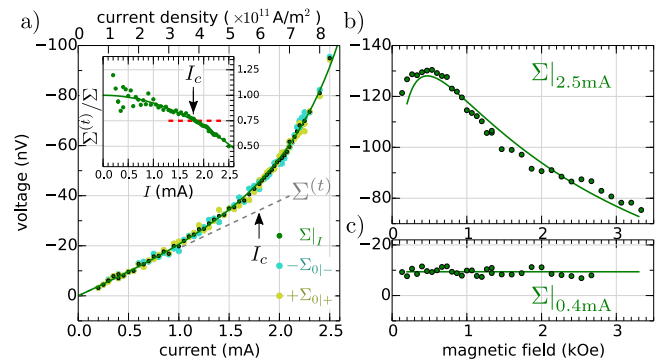

FIG. 3. (Color online) a) Current dependence of the sum signal Σ averaged over the two current polarities. The dashed line, $\Sigma^{(t)}$, is a linear fit of the low current regime. The insert shows the variation of the normalized inverse spin conductance $\Sigma^{(t)}/\Sigma$ as a function of current. The solid line is a parabolic fit of its drop and the arrow indicates the current required to observe a 25% change in normalized conductance. We use it to mark the crossover from a linear to a nonlinear spin transport regime. Variation of Σ as a function of magnetic field for two different current intensities b) above and c) bellow I_c.

linear conductance occurs very gradually and approximately follows a quadratic behavior. Such progressive rise is very different from the sudden surge of magnons number reported before in these systems[2,18]. We have plotted in the insert of FIG.3a the variation of the normalized inverse spin conductance $\Sigma^{(t)}/\Sigma$ as a function of current. The observed drop follows a parabolic behavior (cf. solid line fit). We indicate by an arrow, $I_c = 1.8$ mA ($J_c \approx 6 \times 10^{11}$ A/m^2), the current intensity necessary to change the normalized spin conductance by 25%, chosen as a landmark for the crossover from a linear spin conduction regime to a nonlinear spin conduction regime. Note that J_c is of the same order of magnitude as the threshold current for damping compensation of coherent modes observed at the same applied field ($H_0 = 2$ kOe) in microstructures[16,40,41].

More insight about the nature of the magnons excited above I_c can be obtained by studying the field dependence of Σ[42]. The results are shown in FIG.3b and 3c for two values of the current $I = 0.4$ and 2.5 mA, respectively below and above I_c. While in the field range explored, the signal is almost independent of H_0 when $I < I_c$, it becomes strongly field dependent when $I > I_c$. This different behaviors are consistent with assigning the spin transport to thermal magnons below I_c and mainly to subthermal magnons above I_c. In the former case, the magnons' energy is of the order of the exchange energy, while in the latter case, because of their long wavelength, their energy is of the order of the magnetostatic energy. In consequence, Σ is expected to increase with decreasing field at fixed I, because of the associated decrease of the threshold current for damping compensation. The behavior scales well with the reduced quantity I/I_c. This is shown by the solid line in FIG.3b, which dis-

plays the expected field dependence of $1/I_c(H_0)^{16}$) where $I_c \propto (\omega_H + \omega_M/2)(\alpha + \gamma\Delta H_0/(2\omega_K))$, with $\omega_H = \gamma H_0$ and $\omega_M = 4\pi\gamma M_s$, γ being the gyromagnetic ratio, and $\omega_K = \sqrt{\omega_H(\omega_H + \omega_M)}$ is the Kittel's law. We have used here the amount of inhomogeneous broadening, $\Delta H_0 = 1.5$G (probably position dependent), as an adjustable parameter, while the value of the other parameters are those extracted from Table.1.

The above interpretation has been checked by performing microfocus Brillouin light scattering (μ-BLS) in the sub-thermal energy range on the exact same device as the one used above. FIG.4a and 4b show the spectral distribution of the BLS intensity, J, underneath the injector while rotating the sample in-plane relative to a fixed external magnetic field biased at $H_0 = +2$ kOe. Since this produces a shift in the position of the spot along the Pt wire, the different spectra are normalized by the maximum BLS intensity measured at $I = 0$ (green)^{43}. We first perform BLS spectroscopy by applying the external field parallel to the wires, $i.e.$ along the $\hat{y}$-direction (or $\varphi = \pm90°$), hereby providing a reference spectrum about the out-of-equilibrium magnons distribution produced by Joule heating. The current injected in the wire is $I = 2.5$ mA and we use here the same pulse method. The results are shown in black in the two panels FIG.4a and 4b for respectively positive and negative current pulses. The maximum intensity of these black curve indicates the resonance frequency of the Kittel mode, $\omega_K/(2\pi)$, at the corresponding temperature. This is because the μ-BLS response function is centered around the long wavelength magnons. Indeed, the detected signal decreases once the magnon wavelength is smaller than the spot size (approximately 0.4 μm: diffraction limited). We then turn the magnetic field in the $+\hat{x}$-direction (or $\varphi = 0°$). We show in panel FIG.4a the result for positive current pulses (red) and in panel 4b the result for negative current pulses (blue). The shaded areas on the figures underline the differences with respect to their reference spectra. We clearly observe in FIG.4a a decrease of the number of subthermal magnons around f_K and in FIG.4b their enhancement 0.6 GHz below f_K. The enhancement is observed when $(I \cdot H_0) < 0$ (blue), which corresponds to the configuration where the SOT compensates the damping (cf. convention in FIG1a). In order to isolate the contribution produced solely by SOT, we substract the spectral contribution measured at $+I$ to the one measured at $-I$. We have plotted in FIG4c how the spectral integration of this differential signal $\mathcal{J}_\pm = \int J_\pm d\omega$ varies as a function of the current. One observes a regime of linear rise at small current, followed by a growth above $J_c \approx 6 \times 10^{11}$A/m^2 in a similar fashion as the one reported in FIG3a. The μ-BLS experiment thus provides a direct evidence that an additional spin conduction channel has indeed emerged in the GHz frequency range (subthermal) at large current when SOT is

in the range to compensate the damping.

In summary, we report a study on the spin nonlinear conductance of open YIG films driven by large SOT.
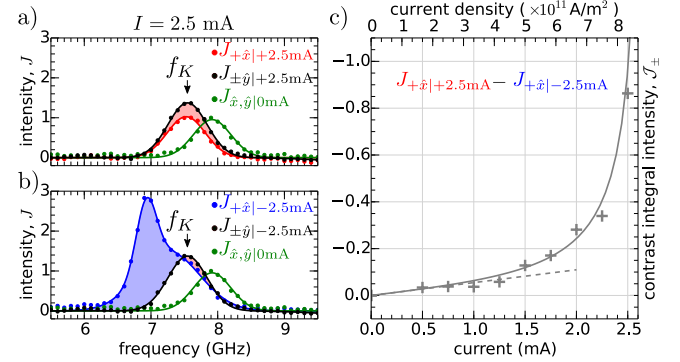

FIG. 4. (Color online) Micro-BLS studies of the subthermal magnons spectrum measured directly underneath the injector at $H_0 = +2$ kOe. Panels a) and b) show the spectral deformation at respectively $I = \pm2.5$ mA when H_0 is oriented in the $+\hat{x}$-direction (azimuthal angle $\varphi = 0°$) comparatively to the $\hat{y}$-direction ($\varphi = \pm90°$). The red/blue area show the magnons annhiliated/created by SOT. The arrows mark the Kittel frequency $f_K = \omega_K/(2\pi)$. Panel c) shows the current evolution of the integrated contrast: difference between magnons annihilated by SOT relative to the ones excited.

While at low values of the spin current, the transport is linear and it seems to be dominated by exchange magnons, at high values of the spin current, the subthermal magnons mainly determine the spin transport leading to a quadratic deviation of the nonlocal voltage. We believe that these findings are not only important from the fundamental point of view, but might be also useful for future applications. While transport of thermal magnons is difficult to control due to their relatively high energies, the crossover to a subthermal spin conduction regime allows the development of controllable spin conductors by relatively weak magnetic fields.

ACKNOWLEDGMENTS

[*] Corresponding author: oklein@cea.fr

[1] S. O. Valenzuela and M. Tinkham, Nature **442**, 176 (2006).

[2] Y. Kajiwara, K. Harii, S. Takahashi, J. Ohe, K. Uchida, M. Mizuguchi, H. Umezawa, H. Kawai, K. Ando, K. Takanashi, S. Maekawa, and E. Saitoh, Nature **464**, 262 (2010).

[3] I. M. Miron, K. Garello, G. Gaudin, P.-J. Zermatten, M. V. Costache, S. Auffret, S. Bandiera, B. Rodmacq, A. Schuhl, and P. Gambardella, Nature **476**, 189 (2011).

[4] J.-C. Rojas-Sánchez, L. Vila, G. Desfonds, S. Gambarelli, J. P. Attan, J. M. D. Teresa, C. Magn, and A. Fert, Nature Comm. **4**, 2944 (2013).

[5] A. R. Mellnik, J. S. Lee, A. Richardella, J. L. Grab, P. J. Mintun, M. H. Fischer, A. Vaezi, A. Manchon, E.-A. Kim, N. Samarth, and D. C. Ralph, Nature **511**, 449 (2014).

[6] S. Sangiao, J. M. De Teresa, L. Morellon, I. Lucas, M. C. Martinez-Velarte, and M. Viret, Appl. Phys. Lett. **106**, 172403 (2015).

[7] J.-Y. Chauleau, M. Boselli, S. Gariglio, R. Weil, G. de Loubens, J.-M. Triscone, and M. Viret, EPL **116**, 17006 (2016).

[8] L. J. Cornelissen, J. Liu, R. A. Duine, J. Ben Youssef, and B. J. van Wees, Nature Phys. **11**, 1022 (2015).

[9] S. T. B. Goennenwein, R. Schlitz, M. Pernpeintner, K. Ganzhorn, M. Althammer, R. Gross, and H. Huebl, Appl. Phys. Lett. **107**, 172405 (2015).

[10] Z. Wang, Y. Sun, M. Wu, V. Tiberkevich, and A. Slavin, Phys. Rev. Lett. **107**, 146602 (2011).

[11] E. Padrón-Hernández, A. Azevedo, and S. M. Rezende, Appl. Phys. Lett. **99**, 192511 (2011).

[12] A. V. Chumak, A. A. Serga, M. B. Jungfleisch, R. Neb, D. A. Bozhko, V. S. Tiberkevich, and B. Hillebrands, Appl. Phys. Lett. **100**, 082405 (2012).

[13] C. Hahn, G. de Loubens, O. Klein, M. Viret, V. V. Naletov, and J. Ben Youssef, Phys. Rev. B **87**, 174417 (2013).

[14] O. d'Allivy Kelly, A. Anane, R. Bernard, J. Ben Youssef, C. Hahn, A. H. Molpeceres, C. Carretero, E. Jacquet, C. Deranlot, P. Bortolotti, R. Lebourgeois, J.-C. Mage, G. de Loubens, O. Klein, V. Cros, and A. Fert, Appl. Phys. Lett. **103**, 082408 (2013).

[15] A. Hamadeh, O. d'Allivy Kelly, C. Hahn, H. Meley, R. Bernard, A. H. Molpeceres, V. V. Naletov, M. Viret, A. Anane, V. Cros, S. O. Demokritov, J. L. Prieto, M. Muñoz, G. de Loubens, and O. Klein, Phys. Rev. Lett. **113**, 197203 (2014).

[16] M. Collet, X. de Milly, O. d'Allivy Kelly, V. Naletov, R. Bernard, P. Bortolotti, J. Ben Youssef, V. Demidov, S. Demokritov, J. Prieto, M. Muñoz, V. Cros, A. Anane, G. de Loubens, and O. Klein, Nature Commun. **7**, 10377 (2016).

[17] V. Lauer, D. A. Bozhko, T. Brcher, P. Pirro, V. I. Vasyuchka, A. A. Serga, M. B. Jungfleisch, M. Agrawal, Y. V. Kobljanskyj, G. A. Melkov, C. Dubs, B. Hillebrands, and A. V. Chumak, Appl. Phys. Lett. **108**, 012402 (2016).

[18] D. Wesenberg, T. Liu, D. Balzar, M. Wu, and B. L. Zink, Nat Phys **advance online publication**, (2017).

[19] S. A. Bender, R. A. Duine, and Y. Tserkovnyak, Phys. Rev. Lett. **108**, 246601 (2012).

[20] V. E. Demidov, S. Urazhdin, E. R. J. Edwards, M. D. Stiles, R. D. McMichael, and S. O. Demokritov, Phys. Rev. Lett. **107**, 107204 (2011).

[21] K. S. Tikhonov, J. Sinova, and A. M. Finkelstein, Nature Comm. **4**, 1945 (2013).

[22] S. O. Demokritov, V. E. Demidov, O. Dzyapko, G. A. Melkov, A. A. Serga, B. Hillebrands, and A. N. Slavin, Nature **443**, 430 (2006).

[23] V. E. Demidov, O. Dzyapko, S. O. Demokritov, G. A. Melkov, and A. N. Slavin, Phys. Rev. Lett. **99**, 037205 (2007).

[24] C. Du, T. van der Sar, T. X. Zhou, P. Upadhyaya, F. Casola, H. Zhang, M. C. Onbasli, C. A. Ross, R. L. Walsworth, Y. Tserkovnyak, and et al., Science **357**, 195198 (2017).

[25] A. A. Serga, V. S. Tiberkevich, C. W. Sandweg, V. I. Vasyuchka, D. A. Bozhko, A. V. Chumak, T. Neumann, B. Obry, G. A. Melkov, A. N. Slavin, and B. Hillebrands, Nature Comm **5**, 3452 (2014).

[26] V. E. Demidov, M. Evelt, V. Bessonov, S. O. Demokritov, J. L. Prieto, M. Muoz, J. Ben Youssef, V. V. Naletov, G. de Loubens, O. Klein, M. Collet, P. Bortolotti, V. Cros, and A. Anane, Sci. Rep. **6**, 32781 (2016).

[27] J. Li, Y. Xu, M. Aldosary, C. Tang, Z. Lin, S. Zhang, R. Lake, and J. Shi, Nature Commun. **7**, 10858 (2016).

[28] H. Wu, C. H. Wan, X. Zhang, Z. H. Yuan, Q. T. Zhang, J. Y. Qin, H. X. Wei, X. F. Han, and S. Zhang, Phys. Rev. B **93**, 060403 (2016).

[29] L. J. Cornelissen, K. J. H. Peters, G. E. W. Bauer, R. A. Duine, and B. J. van Wees, Phys. Rev. B **94**, 014412 (2016).

[30] B. Flebus, P. Upadhyaya, R. A. Duine, and Y. Tserkovnyak, Phys. Rev. B **94**, 214428 (2016).

[31] S. A. Bender and Y. Tserkovnyak, Phys. Rev. B **93**, 064418 (2016).

[32] V. Castel, N. Vlietstra, B. J. van Wees, and J. Ben Youssef, Phys. Rev. B **86**, 134419 (2012).

[33] YIG saturation magnetization decreases by about $4G/^{\circ}C$.

[34] N. Thiery, V. V. Naletov, L. Vila, A. Marty, J.-F. Jacquot, G. de Loubens, M. Viret, A. Anane, V. Cros, J. B. Youssef, V. E. Demidov, S. O. Demokritov, and O. Klein, (to be published) (2017).

[35] H_0 is much higher than the Oersted field of the current (< 50 Oe).

[36] K. Uchida, J. Xiao, H. Adachi, J. Ohe, S. Takahashi, J. Ieda, T. Ota, Y. Kajiwara, H. Umezawa, H. Kawai, G. E. W. Bauer, S. Maekawa, and E. Saitoh, Nature Mater. **9**, 894 (2010).

[37] H. Jin, S. R. Boona, Z. Yang, R. C. Myers, and J. P. Heremans, Phys. Rev. B **92**, 054436 (2015).

[38] C. Safranski, I. Barsukov, H. K. Lee, T. Schneider, A. A. Jara, A. Smith, H. Chang, K. Lenz, J. Lindner, Y. Tserkovnyak, and et al., Nature Communications **8** (2017), 10.1038/s41467-017-00184-5.

[39] The non-local linear resistance between the two Pt wires is $\Sigma^{(t)}/I = 0.019$ mΩ.

[40] M. Evelt, V. E. Demidov, V. Bessonov, S. O. Demokritov, J. L. Prieto, M. Muoz, J. Ben Youssef, V. V. Naletov, G. de Loubens, O. Klein, M. Collet, K. Garcia-Hernandez, P. Bortolotti, V. Cros, and A. Anane, Appl. Phys. Lett. **108**, 172406 (2016).

[41] A more precise comparison of the threshold values should also take into account the different thermalization of YIG underneath the Pt between systems.

[42] L. J. Cornelissen and B. J. van Wees, Phys. Rev. B **93**, 020403 (2016).

[43] We find that the normalized spectra are invariant with respect to a translation of the μ-BLS spot position along the wire direction.